

Appendix A

We show the perturbation method to solve the general abstract equation in the form of $Aw + \lambda w = \lambda e$ where $A: H \rightarrow H$ is a linear continuous self-adjoint operator between some real Hilbert space H with inner product denoted as $\langle \cdot, \cdot \rangle$, $w, e \in H$ and there is a known $w_0 \neq 0$ such that $Aw_0 = 0$, i.e., A has an eigenvalue 0. We show how w behaves when $\lambda \rightarrow 0$. We assume that w can be expanded in the power series of λ as $w = Cw_0 + \lambda w_1 + \lambda^2 w_2 + \dots$ where C is a constant independent of λ , and w_1, w_2, \dots are unknown functions. Then we substitute this expansion into the original equation:

$A(Cw_0 + \lambda w_1 + \lambda^2 w_2 + \dots) + \lambda(Cw_0 + \lambda w_1 + \lambda^2 w_2 + \dots) = \lambda e$. For λ^0 -order terms: $Aw_0 = 0$ is trivial. For λ^1 -order terms, $Aw_1 + Cw_0 = e$. Finally for λ^2 -order terms, $Aw_2 + w_1 = 0$. Taking inner product with w_0 , it yields: $\langle Aw_1, w_0 \rangle + C \langle w_0, w_0 \rangle = \langle e, w_0 \rangle$, and by self-adjointness, $\langle Aw_1, w_0 \rangle = \langle w_1, Aw_0 \rangle = \langle w_1, 0 \rangle = 0$.

Thus $C = \langle e, w_0 \rangle / \langle w_0, w_0 \rangle$. To obtain w_1 , we need to solve equation

$$Aw_1 = e - \langle e, w_0 \rangle / \langle w_0, w_0 \rangle \cdot w_0. \quad (S1)$$

Eq. (S1) has non-unique solutions. But by taking the inner product of the equation $Aw_2 + w_1 = 0$, it yields:

$$\begin{aligned} 0 &= \langle Aw_2, w_0 \rangle + \langle w_1, w_0 \rangle \\ &= \langle w_2, Aw_0 \rangle + \langle w_1, w_0 \rangle = \langle w_1, w_0 \rangle. \end{aligned}$$

Thus w_1 is determined uniquely by this condition $\langle w_1, w_0 \rangle = 0$.

Note that if λe is replaced by e ($\neq 0$) without the small λ , the resulting equation $Aw + \lambda w = e$ has quite distinct behavior as $\lambda \rightarrow 0$. In this case $w \sim Cw_0$ where $C(\lambda)$ is depending on λ and $C \rightarrow \infty$ as $\lambda \rightarrow 0$ by

$$\begin{aligned} \langle e, w_0 \rangle &= \langle Aw + \lambda w, w_0 \rangle = \langle Aw, w_0 \rangle + \lambda \langle w, w_0 \rangle \\ &= \langle w, Aw_0 \rangle + \lambda \langle w, w_0 \rangle = \lambda \langle w, w_0 \rangle \sim \lambda \langle Cw_0, w_0 \rangle \end{aligned}$$

and the explicit expression for C is thus $C = \lambda^{-1} \langle w_0, e \rangle / \langle w_0, w_0 \rangle$.

Appendix B.

We derive the governing equation:

$$\begin{aligned} M_1 + 1/8 \cdot p(4R_1^2 - t_1^2) - pR_1 w_1 &= C, \\ M_2 + 1/8 \cdot p(4R_2^2 - t_2^2) - pR_2 w_2 &= C \end{aligned}$$

where M_i, w_i, t_i, R_i are cross-section resultant moments about the point of middle axis, radial displacements, thicknesses and middle axis radius at point s where $i=1$ represents the corroded region and $i=2$ represents the intact region with C being an unknown constant.

Step 1. Assuming small tangential displacements and radial displacements (Assumption (1)), the curvature change at s is represented linearly as $1/R_i^2 (w_i'' + v_i')$ and the membrane strains are $1/R_i \cdot (dv_i/ds - w_i)$.

If both curvature change and membrane strain are zero, the related displacements are related to rigid-body motion. In that case the curvature change and membrane strain should vanish: $v_i' = w_i, w_i'' + v_i' = 0$. Substituting the first equation into the second, it yields: $w_i'' + w_i = 0$. Thus $w_i = a_i \sin s + b_i \cos s$.

Then substituting this w_i back to the first equation, it leads to $v_i = -a_i \cos s + b_i \sin s + c_i$ for some real a_i, b_i, c_i .

The geometric meaning of c_i is some small rigid-body rotation around origin point. a_i is the horizontal rigid-body translation and b_i is the vertical rigid-body translation.

Since the deformation is assumed to be symmetric, both rotational and horizontal translational rigid-body motion are excluded. But arbitrary vertical translation is allowed.

Step 2. We make an essential assumption (2) here that the membrane compressive force N_i during deformation can be approximately represented by $N_i = p(R_i + t_i / 2 + o(1))$ where $o(1)$ is some term much smaller than unity.

This assumption (2) is based on the observation that when curvature change is small (since displacements are small), the circular segment remains almost circular and thus the circular segment's membrane behavior should resemble the of a uniform ring. Note that for a uniform ring with middle axis radius R_i and thickness t_i under pressure p , the membrane force is just $p(R_i + t_i / 2)$. And our assumption (2) is just equivalent to the assumption that the membrane force of corroded ring in each uniform segment (corroded region and intact region) during deformation should be approximate to that of some uniform ring with some unknown but small error term $o(1)$. It is important to note that all displacements are assumed to be small in this paper and this assumption (1) is made based on the fact that in practical engineering the steel pipeline reaches critical collapse value when displacements are very small since the elastic modulus of steel is very large. The last assumption (3) is the conventional Euler-Bernoulli beam assumption asserting that the cross-section is not deformed and lines perpendicular to middle axis remain perpendicular. There are no other theoretical assumptions other than assumptions (1), (2), (3). All results are derived rigorously by these three assumptions. The calculation results under these assumptions are verified by some comparisons with FEA results in Section. 3 and also in Appendix G for stress.

We can always superimpose some vertical rigid-body translation without affecting the force balance and moment balance. Thus we may assume particularly without loss of generality after some such superimposition at point $s=0$, the membrane compressive force is: $N_1|_{s=0} = p(R_1 + t_1 / 2 - w_1(0))$. To be more specific: if during deformation at point $s=0$, the membrane force is $N_1|_{s=0} = p(R_1 + t_1 / 2 + o(1))$ then the radial displacement w_1 at $s=0$ is \bar{w} . Then we superimpose a vertical rigid-body translation by $b_1 = -o(1) - \bar{w}$ and define

$$\begin{aligned}\hat{w}_1 &= b_1 \cos s + w_1, \\ \hat{v}_1 &= b_1 \sin s + v_1, \\ \hat{w}_2 &= b_1 \cos s + w_2, \\ \hat{v}_2 &= b_1 \sin s + v_2\end{aligned}$$

as the new displacement field. $-\hat{w}_1(0) = -(b_1 + \bar{w}) = -(-o(1) - \bar{w} + \bar{w}) = o(1)$.

And then with this new radial displacement field \hat{w}_1 , $N_1|_{s=0} = p(R_1 + t_1 / 2 - \hat{w}_1(0))$. Thus there is indeed no loss of generality.

Step 3. Fig.S1 shows the schematic of force and moment of the deformed segment where C point is the middle axis point at $s=0$. B point is the outer point at $s=0$. E point is a middle axis point in intact region with angular coordinate s and D is the outer point at s . p is the external pressure acting on the outer boundary. Euler-Bernoulli beam assumption is adopted here, i.e., cross-section is not deformed and cross-section remains perpendicular to the deformed middle axis after deformation. Denote \vec{X}_E as the position vector of point E and explicitly we have:

$$\vec{X}_E = (X_1, X_2) = (R_2 \sin s - w_2 \sin s + v_2 \cos s, R_2 \cos s - w_2 \cos s - v_2 \sin s). \quad (S2)$$

A tangent vector at E along the deformed middle axis is $\vec{t} = (dX_1 / ds, dX_2 / ds)$ and the unit outer normal vector \vec{n} at point s can be represented as:

$$\vec{n} = \frac{1}{\|\vec{t}\|_2} \cdot (-dX_2 / ds, dX_1 / ds) \quad (S3)$$

where $\|\vec{t}\|_2$ means the vector length of \vec{t} . The point D has position vector as $\vec{X}_D = \vec{X}_E + \vec{n}t_2 / 2$ (since cross-section is not deformed by the Euler-Bernoulli assumption). The point B has position vector as $\vec{X}_B = (0, R_1 + t_1 / 2 - w_1(0))$.

Considering the moment balance around point E , there are four components: moment by membrane compression $N_1|_{s=0}$, moment by external pressure, cross-section moments $M_1|_{s=0}$ and $M_2(s)$. The external pressure can be equivalently represented as a concentrated force acting at middle point of straight line segment BD with magnitude $p|BD|$ (so implicitly pressure remains normal to the outer boundary during deformation and p is indeed a follower load although the cross-section normal rotation is small). The moment from p around point E is thus: $p(\vec{X}_D + \vec{X}_B / 2 - \vec{X}_E) \cdot (\vec{X}_D - \vec{X}_B)$.

The compressive force's moment is then ph where:

$$h = (R_1 + t_1 / 2 - w_1(0)) \cdot (R_1 - w_1(0) - (R_2 \cos s - w_2 \cos s - v_2 \sin s)).$$

Adding them all together, linearizing the resulting equation and dropping the higher order terms, it yields:

$$M_1|_{s=0} + 1/8 \cdot p(4R_1^2 - t_1^2) - pR_1w_1(0) = M_2(s) + 1/8 \cdot p(4R_2^2 - t_2^2) - pR_2w_2(s).$$

We note that the left-hand side is a constant independent of s , thus the right-hand side is a constant. If E lies in the corroded region, the identical derivation gives that:

$$M_1|_{s=0} + 1/8 \cdot p(4R_1^2 - t_1^2) - pR_1w_1(0) = M_1(s) + 1/8 \cdot p(4R_1^2 - t_1^2) - pR_1w_1(s).$$

Thus we conclude that for some constant C :

$$M_1(s) + 1/8 \cdot p(4R_1^2 - t_1^2) - pR_1w_1(s) = C; M_2(s) + 1/8 \cdot p(4R_2^2 - t_2^2) - pR_2w_2(s) = C \quad (S4)$$

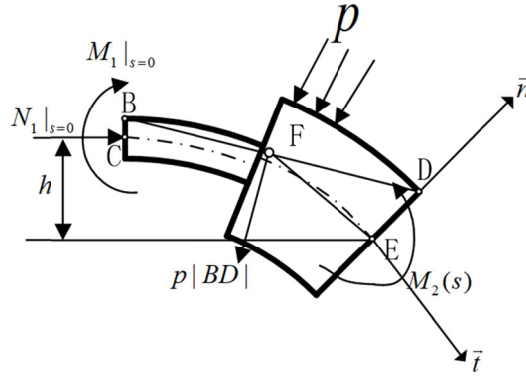


Fig. S1 Force and moment of deformed segment

Appendix C.

This appendix C shows the derivation of continuity condition Eq.(5) by rigorous adoption of the Euler-Bernoulli assumption. Considering an original circular ring of radius R parametrized by angular coordinate s with radial displacement field w , tangential displacement field v of middle axis and another radial coordinate z ($z = 0$ means the middle axis, see Fig.S2).

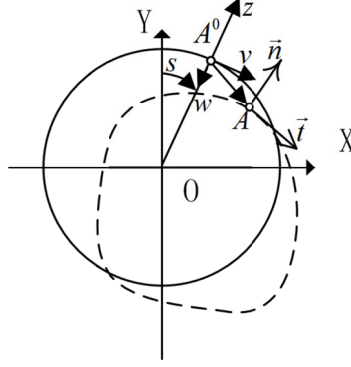


Fig. S2 Kinematics of circular ring

We consider a thickness point at cross-section s with $z \neq 0$ with circumferential displacement $v(s,z)$ and radial displacements $w(s,z)$ and of course $v(s,0) = v(s)$ and $w(s,0) = w(s)$ are the middle axis point's circumferential and radial displacements. An original middle axis point A^0 at s and $z = 0$ moves to a point A with position vector

$$\vec{X}_A = (R \sin s - w(s) \sin s + v(s) \cos s, R \cos s - w(s) \cos s - v(s) \sin s).$$

The tangent vector is then

$$\begin{aligned} d\vec{X}_A / ds = & (R \cos s - v(s) \sin s - w(s) \cos s + v'(s) \cos s - w'(s) \sin s, \\ & -R \sin s - v(s) \cos s + w(s) \sin s - v'(s) \sin s - w'(s) \cos s) \end{aligned} \quad (S5)$$

and unit tangent vector is $\vec{t} = d\vec{X}_A / ds / \|d\vec{X}_A / ds\|_2$. Unit outer normal can be explicitly represented:

$$\begin{aligned} \vec{n} = & \left\{ \frac{R \sin[s] + \cos[s]v[s] - \sin[s]w[s] + \sin[s]v'[s] + \cos[s]w'[s]}{\sqrt{R^2 + v[s]^2 + w[s]^2 + 2Rv'[s] + v'[s]^2}}, \right. \\ & \left. \frac{R \cos[s] - \sin[s]v[s] - \cos[s]w[s] + \cos[s]v'[s] - \sin[s]w'[s]}{\sqrt{R^2 + v[s]^2 + w[s]^2 + 2Rv'[s] + v'[s]^2}} \right\}, \end{aligned} \quad (S6)$$

By linearization, $\vec{n} \approx \vec{N} + \theta \vec{T}$ where $\vec{N} = (\sin s, \cos s)$, $\vec{T} = (\cos s, -\sin s)$ are defined and $\theta = (v + w') / R$. For thickness point with coordinates (s, z) , its original position vector is $\vec{x}(s, z) = ((R + z) \sin s, (R + z) \cos s)$.

By Euler-Bernoulli assumption, its position vector is $\vec{X}(s, z) = \vec{X}_A(s) + \vec{n} \cdot z$. The tangential displacement at point (s, z) is just:

$$v(s, z) = (\vec{X}(s, z) - \vec{x}(s, z)) \cdot \vec{T}(s). \quad (S7)$$

And radial displacement of point (s, z) is just:

$$w(s, z) = (\vec{X}(s, z) - \vec{x}(s, z)) \cdot (-\vec{N}(s)). \quad (S8)$$

Linearization of Eq.(5) and Eq.(8) leads to $v(s, z) = v(s) + (v(s) + w'(s)) / R \cdot z$ and $w(s, z) = w(s)$.

Then returning to the context of section 2.2 at s_1 , $w_1(s_1) = w_1(s_1, R_2 - R_1) = w_2(s_1)$ and

$$\begin{aligned} v_2(s_1) = v_1(s_1, R_2 - R_1) = v_1(s_1) + \frac{v_1(s_1) + w_1'(s_1)}{R_1} \cdot (R_2 - R_1); \\ v_1(s_1) = v_2(s_1, R_1 - R_2) = v_2(s_1) + \frac{v_2(s_1) + w_2'(s_1)}{R_2} \cdot (R_1 - R_2). \end{aligned} \quad (S9)$$

This equation directly implies that:

$$(v_1(s_1) + w_1'(s_1)) / R_1 = (v_2(s_1) + w_2'(s_1)) / R_2. \quad (S10)$$

Note that this equation just means that the rotation of cross-section is identical. By the first equation of Eq.(S9), after some calculation, $v_1(s_1) / R_1 - v_2(s_1) / R_2 = w_1'(s_1)(1 / R_2 - 1 / R_1)$ and

comparison of this equation with Eq.(S10) yields that $w'_1(s_1) = w'_2(s_1)$. Then the inextensible condition yields:

$$v_1(s_1) - v_1(0) = \int_{[0,s_1]} w_1; v_2(\pi) - v_2(s_1) = \int_{[s_1,\pi]} w_2.$$

By symmetry of deformation, $v_1(0) = v_2(\pi) = 0$ and leads to Eq.(5) directly.

Appendix D.

Here we present the solution of initial slope problem in section 2.4 and we only solve for the extensible model since the inextensible model (although simpler) does not yield the correct initial slope when comparison with FEA results in Section 3 is made. For simplicity, we adopt the simpler continuity conditions in Eq.(6). With the solution strategy outlined in Appendix A, we assume perturbative expansion as:

$$\begin{aligned} w_1 &= c\bar{w}_{01} + p\bar{w}_{11} + p^2\bar{w}_{31} + \dots \\ w_2 &= c\bar{w}_{02} + p\bar{w}_{12} + p^2\bar{w}_{32} + \dots \\ C &= c\bar{C}_0 + p\bar{C}_1 + p^2\bar{C}_2 + \dots \end{aligned} \quad (S11)$$

where \bar{w}_{01} , \bar{w}_{02} , \bar{C}_0 denote the eigenfunctions for the homogeneous equation when $p = 0$, c is a constant independent of p and $\bar{w}_{11}, \dots, \bar{w}_{12}, \dots$ are functions on $[0, \pi]$. And of course $\bar{w}_{01} = \cos s, \bar{w}_{02} = \cos s$ with $\bar{C}_0 = 0$ is the eigenfunction of related homogeneous equation system:

$$w_1'' + w_1 - CR_1^2 / EI_1 = w_2'' + w_2 - CR_2^2 / EI_2 = 0$$

under conditions

$$w_1'(0) = w_2'(\pi) = w_1(s_1) - w_2(s_1) = w_1'(s_1) - w_2'(s_1) = \int_{[0,s_1]} w_1 + \int_{[s_1,\pi]} w_2 = 0..$$

Substitution of this expansion yields the equation systems for the p^1 order terms:

$$(\bar{w}_{11}'' + \bar{w}_{11}) + R_1^3 / EI_1 \cdot c\bar{w}_{01} = \bar{C}_1 R_1^2 / EI_1 + R_1(R_1 + t_1 / 2) / Et_1 - 1 / 8 \cdot R_1^2 / EI_1 \cdot t_1^2 - 4R_1^2); \quad (S12)$$

$$(\bar{w}_{12}'' + \bar{w}_{12}) + R_2^3 / EI_2 \cdot c\bar{w}_{02} = \bar{C}_1 R_2^2 / EI_2 + R_2(R_2 + t_2 / 2) / Et_2 - 1 / 8 \cdot R_2^2 / EI_2 \cdot (t_2^2 - 4R_2^2); \quad (S13)$$

$$\int_{[0,s_1]} \bar{w}_{11} + \int_{[s_1,\pi]} \bar{w}_{12} = R_1(R_1 + t_1 / 2) / Et_1 \cdot s_1 + R_2(R_2 + t_2 / 2) / Et_2 \cdot (\pi - s_1). \quad (S14)$$

Integrate Eq.(S12) from 0 to s_1 and Eq.(S13) from s_1 to π , sum the results and apply the continuity conditions and boundary conditions. We get that:

$$\bar{C}_1 = H_1 c + H_2 \quad (S15)$$

where

$$\begin{aligned} H_1 &= \frac{R_1^3 / EI_1 \cdot \int_{[0,s_1]} \bar{w}_{01} + R_2^3 / EI_2 \cdot \int_{[s_1,\pi]} \bar{w}_{02}}{\frac{R_1^2}{EI_1} \cdot s_1 + \frac{R_2^2}{EI_2} \cdot (\pi - s_1)}; \\ H_2 &= \frac{\frac{s_1}{8} \cdot \frac{R_1^2}{EI_1} \cdot (t_1^2 - 4R_1^2) + \frac{\pi - s_1}{8} \cdot \frac{R_2^2}{EI_2} \cdot (t_2^2 - 4R_2^2)}{\frac{R_1^2}{EI_1} \cdot s_1 + \frac{R_2^2}{EI_2} \cdot (\pi - s_1)}. \end{aligned} \quad (S16)$$

Then multiply Eq.(S12) by $\bar{w}_{01} = \cos s$, integrate it from 0 to s_1 and similarly multiply Eq.(S13) by $\bar{w}_{02} = \cos s$, integrate it from s_1 to π . Then summing up these two integrals and applying the boundary conditions and continuity conditions, it yields an expression for c :

$$c = \frac{\{H_2 R_1^2 / EI_1 + R_1(R_1 + t_1 / 2) / Et_1 - 1 / 8 \cdot R_1^2 / EI_1 \cdot (t_1^2 - 4R_1^2)\} \int_{[0, s_1]} \bar{w}_{01} + \{H_2 R_2^2 / EI_2 + R_2(R_2 + t_2 / 2) / Et_2 - 1 / 8 \cdot R_2^2 / EI_2 \cdot (t_2^2 - 4R_2^2)\} \int_{[s_1, \pi]} \bar{w}_{02}}{[R_1^3 / EI_1 \cdot \int_{[0, s_1]} \bar{w}_{01}^2 + R_2^3 / EI_2 \cdot \int_{[s_1, \pi]} \bar{w}_{02}^2 - H_1 R_1^2 / EI_1 \cdot \int_{[0, s_1]} \bar{w}_{01} - H_1 R_2^2 / EI_2 \cdot \int_{[s_1, \pi]} \bar{w}_{02}]}. \quad (S17)$$

Then we calculate for p^2 order terms:

$$\bar{w}_{21}'' + \bar{w}_{21} + R_1^3 / EI_1 \cdot \bar{w}_{11} = \bar{C}_2 R_1^2 / EI_1; \quad (S18)$$

$$\bar{w}_{22}'' + \bar{w}_{22} + R_2^3 / EI_2 \cdot \bar{w}_{12} = \bar{C}_2 R_2^2 / EI_2.$$

$$\begin{aligned} \bar{w}_{21}'(0) = \bar{w}_{22}'(\pi) = 0, \bar{w}_{21}(s_1) - \bar{w}_{22}(s_1) \\ = \bar{w}_{21}'(s_1) - \bar{w}_{22}'(s_1) = 0; \int_{[0, s_1]} \bar{w}_{21} + \int_{[s_1, \pi]} \bar{w}_{22} = 0. \end{aligned} \quad (S19)$$

By similar integration,

$$\bar{C}_2 = \frac{R_1^3 / EI_1 \cdot \int_{[0, s_1]} \bar{w}_{11} + R_2^3 / EI_2 \cdot \int_{[s_1, \pi]} \bar{w}_{12}}{R_1^2 / EI_1 \cdot s_1 + R_2^2 / EI_2 \cdot (\pi - s_1)}. \quad (S20)$$

Then multiplying the equations in Eq. (S18) with \bar{w}_{01} and \bar{w}_{02} , taking integration and summing them up similarly, we find the orthogonality condition:

$$R_1^3 / EI_1 \cdot \int_{[0, s_1]} \bar{w}_{11} \bar{w}_{01} + R_2^3 / EI_2 \cdot \int_{[s_1, \pi]} \bar{w}_{12} \bar{w}_{02} = \bar{C}_2 R_1^2 / EI_1 \int_{[0, s_1]} \bar{w}_{01} + \bar{C}_2 R_2^2 / EI_2 \int_{[s_1, \pi]} \bar{w}_{02}. \quad (S21)$$

Eq.(S21) and Eq.(S20) represent a necessary condition to be imposed on \bar{w}_{11} and \bar{w}_{12} . Then we solve for \bar{w}_{11} and \bar{w}_{12} now. To simplify the notation, define

$$G_1 = \bar{C}_1 R_1^2 / EI_1 + R_1(R_1 + t_1 / 2) / Et_1 - 1 / 8 \cdot R_1^2 / EI_1 \cdot (t_1^2 - 4R_1^2); P_1 = -R_1^3 / EI_1 \cdot c.$$

$$G_2 = \bar{C}_1 R_2^2 / EI_2 + R_2(R_2 + t_2 / 2) / Et_2 - 1 / 8 \cdot R_2^2 / EI_2 \cdot (t_2^2 - 4R_2^2); P_2 = -R_2^3 / EI_2 \cdot c.$$

The general solution is then:

$$\begin{aligned} \bar{w}_{11} &= G_1 + \left(\frac{P_1}{2} + a_1\right) \cos s + \left(\frac{P_1 s}{2} + b_1\right) \sin s; \\ \bar{w}_{12} &= G_2 + \left(\frac{P_2}{2} + a_2\right) \cos s + \left(\frac{P_2 s}{2} + b_2\right) \sin s \end{aligned} \quad (S22)$$

where a_1, b_1, a_2, b_2 are constants from integration. Then we require these solutions to satisfy the following conditions:

$$\bar{w}_{11}'(0) = \bar{w}_{11}'(s_1) - \bar{w}_{12}'(s_1) = \bar{w}_{11}(s_1) - \bar{w}_{12}(s_1) = 0 \quad (S23)$$

and the orthogonal condition by Eq.(S20) and Eq.(S21). There are four conditions and four unknowns a_1, a_2, b_1, b_2 , thus a linear equation can be solved to obtain a_1, a_2, b_1, b_2 . The reader may wonder why we drop the boundary condition $\bar{w}_{12}(\pi) = 0$: this is because this boundary condition is not necessary and can be verified to be automatically satisfied when \bar{w}_{11} and \bar{w}_{12} are obtained.

Appendix E.

In this appendix E, we discuss the effect of convergence parameters c_0 and generally the homotopy analysis method (Liao, 2012; Chen et al., 2021) leads to an equation:

$$(1 - \varepsilon)w'' - c_0 \varepsilon(w'' + Qw) = 0 \quad (S24)$$

where Q is an arbitrary fixed function on $[0, \pi]$, c_0 is the so-called convergence parameter to control the convergence of power series: $w = w_0 + \varepsilon w_1 + \varepsilon^2 w_2 + \dots$ and boundary conditions are specified to make this problem well-defined:

$$w_i|_{s=0} = w_0|_{s=0}, w_i'|_{s=0} = w_0'|_{s=0}, \forall i \geq 1.$$

We can substitute this expansion into the equation and use the boundary conditions to eliminate the integration constants. We find that:

$$w_1(s) = (1 + c_0)(w_0(s) - w_0|_{s=0} - w_0'|_{s=0} \cdot s) + \int_{[0,s]} \int_{[0,s]} c_0 Q(\tau) w_0(\tau) d\tau ds. \quad (S25)$$

$$w_i(s) = (1 + c_0)w_{i-1}(s) + \int_{[0,s]} \int_{[0,s]} c_0 Q(\tau) w_{i-1}(\tau) d\tau ds; i \geq 2. \quad (S26)$$

If $Q = 0$, then $w_i(s) = (1 + c_0)w_{i-1}(s)$ leads to a geometric power series so that the power series converges if and only if $|1 + c_0| < 1$. Thus we may only expect the convergence when $|1 + c_0| < 1$ ($c_0 = -1$ is of course lying in this domain). We can show $|1 + c_0| < 1$ is indeed enough for convergence when $\varepsilon = 1$. Since by division we obtain $w'' + \frac{-c_0\varepsilon}{1 - \varepsilon - c_0\varepsilon} Qw = 0$, and by collecting $c_0\varepsilon / (1 - \varepsilon - \varepsilon c_0)$ as h , it leads to $w'' = hQw$. It has been shown that $w(s)$ (depending on real number h) is analytic for $-\infty < h < \infty$ by Inequality 20. Thus we may regard $w(s)$ as an analytic function of h and h can also be regarded as a function of ε . From basic functional analysis, it is well-known that composition of two analytic functions are analytic on certain domain and of course $h(\varepsilon) = c_0\varepsilon / (1 - \varepsilon(1 + c_0))$ is analytic for $|\varepsilon| < 1/|1 + c_0|$. Since only convergence at $\varepsilon = 1$ is required, thus $1/|1 + c_0| > 1$ (i.e., $c_0 \in (0, -2)$) suffices to guarantee the convergence. From this discussion, we show that setting $c_0 \neq -1$ leads to smaller convergence radius and thus there is no necessity to set c_0 to a number $c_0 \neq -1$. For $c_0 = 0$, the integral term in Eq.(S26) vanishes and $w_i = w_{i-1}$ for any $i \geq 2$. Thus unless $w_2 = 0$ identically, the resulting series $w = w_0 + w_1 + \dots$ must be diverging.

Let us present an example to verify this discussion. As an example, set $w_0 = 1 + s$ and $Q = 1 + s$, then we can calculate w_i by Eq.(S26) and Eq.(S25). We would check the convergence of truncated series $w_1 + \dots + w_m$ when m is going to infinity. To check the divergence/convergence critical values $c_0 = 0, -2$, we calculate truncated w for $c_0 = -0.1$ and $0.1, -1.7, -1.9$ and -2.05 in Fig.S14, Fig.S15, Fig.S16, Fig.S17 and Fig.S18 respectively. In Fig.S14, at $c_0 = -0.1$, when $m = 40, 50, 60$, the curves converge. However when c_0 is slightly higher than 0.0 , at $c_0 = 0.1$, the divergence is rapid. Slow convergence and extremely slow convergence are observed for $c_0 = -1.7$ and -1.9 , but rapid divergence is observed when c_0 is slightly lower than $c_0 = -2.0$. These verify the conclusion that $c_0 \in (-2, 0)$ guarantees the convergence. This appendix serves to enhance the understanding of the controlling parameter in the so-called homotopy analysis method (Chen et al., 2021).

Appendix F.

We present the shooting method combined with Newton-Raphson iteration to numerically solve Eq.(10) and Eq.(11). This method firstly converts the problem into an equivalent initial value problem. To solve Eq.(10) we define

$$y_1(x) = w(x), y_2 = w'(x), y_3(x) = \int_{[0,x]} w(x) dx$$

and Eq.(10) is equivalent to:

$$\begin{aligned} y_1'(x) &= y_2(x); \\ y_2'(x) &= CR(x)^2 / EI(x) - y_1(x) - pR(x)^3 / EI(x) \cdot y_1(x) \\ &\quad - 1/8 \cdot pR(x)^2 / EI(x) \cdot (t(x)^2 - 4R(x)^2); \\ y_3'(x) &= y_1(x). \end{aligned}$$

where C is an unknown constant. Then boundary conditions lead to $y_2(0) = 0, y_3(0) = 0, y_2(\pi) = 0$ and $y_3(\pi) = 0$. The initial condition $y_1(0) = c$ (denoted as c) is unknown and thus

there are two unknowns c and C with two constraints $y_2(\pi) = 0$ and $y_3(\pi) = 0$ at end point $x = \pi$. For each p fixed, an initial guess for C, c would be prescribed; then by this initially guessed C, c , this initial value problem can be solved by the Runge-Kutta method by ODE45 solver in Matlab software (denoted as original calculation), i.e., for each c, C , we can obtain the values $y_2(\pi)$ and $y_3(\pi)$; if $y_2(\pi) \approx 0$ and $y_3(\pi) \approx 0$ with small error, we are done and these C, c are the required solution; otherwise we can replace (C, c) by perturbed $(C + \delta, c)$ and (C, c) by perturbed $(C, c + \delta)$ where δ is a very small perturbing value, e.g., $1e-4$ to carry out second and third calculations respectively by the Runge-Kutta method; denote the value $y_2(\pi)$ and $y_3(\pi)$ by original calculation as $y_2(\pi)|_0, y_3(\pi)|_0$ and similarly $y_2(\pi)|_1, y_3(\pi)|_1$ in second calculation, $y_2(\pi)|_2, y_3(\pi)|_2$ in third calculation; then an approximately Jacobian matrix is formed:

$$J = \frac{1}{\delta} \begin{bmatrix} y_2(\pi)|_1 - y_2(\pi)|_0 & y_2(\pi)|_2 - y_2(\pi)|_0 \\ y_3(\pi)|_1 - y_3(\pi)|_0 & y_3(\pi)|_2 - y_3(\pi)|_0 \end{bmatrix},$$

$[C, c]$ is updated as $[C, c] + J^{-1} \cdot [-y_2(\pi)|_0, -y_3(\pi)|_0]$; repeat the above Newton-Raphson iteration until convergence is attained for such value of p and then increment p to repeat the above process again. The method to solve Eq.(11) is similar and thus omitted.

Appendix G.

In this appendix G, we use the elastic solution in this paper and initial yielding criterion or the full plastic criterion (Fatt, 1999) to assess the critical collapse pressure of corroded pipes. And a comparison to FEA results is included when plasticity is considered. To simplify the discussion, we assume **elastic-perfectly plastic** material model with yielding stress $\sigma_y = 240 \text{MPa}$. We fix parameters $R_2 = 1 \text{m}$, $E = 200 \text{GPa}$, $t_2 = 0.1R_2$ (thick enough such that plasticity effect cannot be neglected, see also the work (Yan et al., 2016)) as in Section 3.2 and Riks step by Abaqus software is carried out while external pressure is imposed on outer boundary (Nlgeom option is On to account for the large deformation effect, so that pressure is modelled as a follower load). We find excellent prediction capability of maximum stress by our formulation if no yielding happens (here we use the extensible model). Firstly theoretically at each cross-section at s , the circumferential stress is the sum of bending stress and membrane stress and the absolute value of maximum stress at cross-section of s can be represented explicitly by

$$\sigma_i(s) = Et_i / (2R_i^2) \cdot |w_i'' + v_i'| + p(R_i + t_i / 2) / t_i, i = 1, 2 \quad (\text{S27})$$

where $v_i' = -pR_i(R_i + t_i / 2) / (Et_i) + w_i$ for $i = 1, 2$ as in Eq.(3).

Case (1). We first present results when $e = 0$ (symmetric case). Fig.S3 shows how the maximum stress $\sigma(s)$ changes when pressure is increasing by theoretical formulation where $\sigma(s) = \sigma_1(s)$ if $s \in [0, s_1]$ and $\sigma(s) = \sigma_2(s)$ if $s \in (s_1, \pi]$. Due to smaller thickness, when $s < s_1 = \pi / 6 \approx 0.5$, stress is significantly larger than the stress in intact region where $s > s_1$. There is an abrupt stress drop at $s = s_1$. As p increases as 2, 4, 6, 8, 10, 11.53 MPa, the stress increases. We just record that when $p = 11.53$, the maximum stress $\sigma(s)$ has maximum value 240.14 MPa (approximately the same as the specified yielding stress 240 MPa). For the corresponding FEA results, Fig.S4 shows the Mises stress distribution when $p = 11.7077$ MPa (the maximum pressure in load-displacement path). Please note that the maximum Mises stress is indeed 240 MPa by using Abaqus "probe stress value" functionality (the same as the yielding stress) and the number 256.6 MPa in the left box should not be taken as the maximum stress (this somewhat misleading number may be due to some visualization algorithm through data

interpolation or extrapolation in Abaqus and this point applies to Fig.S8 also). If initial yielding criterion is used, the theoretical critical collapse pressure is 11.53MPa and this is very close to the FEA collapse pressure 11.70MPa. FEA stress is also abruptly dropping at $s = s_1$. Moreover FEA offers a good chance to see how plasticity affects the stress when collapse pressure is approached: since by theoretical calculation in Fig.S3 the maximum stress 240.14MPa is attained at $s = 0$, we extract the circumferential stress by using "stress linearization" functionality in Abaqus into Fig. S5. In Fig.S5, circumferential stress is extracted through the stress extraction path (see subplot in Fig.S5) for all points in cross-section of $s = 0$ and $x \in (0, t_1)$ denotes the location of points. When $p = 11.0995 \text{ MPa}$, the yielding stress is slightly smaller than yielding stress 240MPa and the stress distributes as a straight line with maximum absolute value about 237MPa at $x = 0$ and minimum absolute value about 215MPa at $x = t_1$. However when Pa, for small x , the stress becomes a constant around 240MPa (please note that circumferential stress extremely slightly differs from von-Mises stress by the existence of very small radial and shear stress). And when $p = 11.5513 \text{ MPa}$, when $x/t_1 < 0.4$, the stress is almost constant and slightly larger than 240MPa. Finally when $p = 11.7077 \text{ MPa}$ (collapse pressure), for $x/t_1 < 0.8$, the stress is almost constant. This clearly shows how the plastic region "propagates" in the thickness direction after yielding and the collapse pressure is reached when this region "occupies" 80% of thickness. But it is still interesting to note that, even so, the initial yielding criterion leads to a very close critical pressure prediction when FEA result is compared (see Table.S1). But situations are quite different for $e = 1$ in the following.

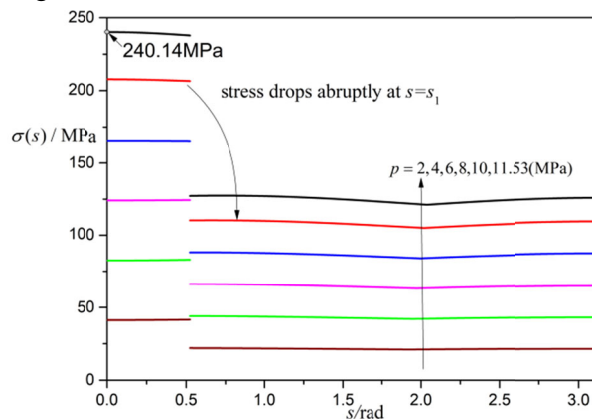


Fig. S3 Distribution of stress when $e=0$ (theoretical)

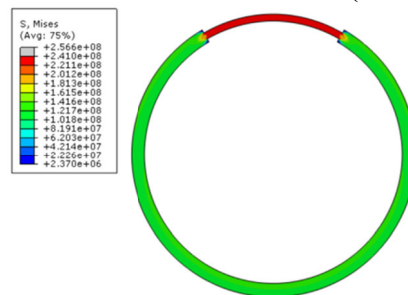


Fig. S4 Stress when maximum pressure occurs for $e=0$

Case (2). Fig.S6 shows the circumferential stress variation (from FEA) for various pressures and also the theoretical stress at $s=0$ (theoretical stress is a linear combination of bending stress and membrane stress and thus forms a straight line, see solid lines in Fig.S6) is calculated by our formulation and compared with FEA results (see discrete symbol lines). All theoretical stresses agree well with the FEA results, however, when p is larger than 8.03MPa, yielding occurs and the similar pattern of "propagating" plastic region is observed when p is further increasing.

The FEA collapse pressure about 10.43MPa is reached when the plastic region occupies also about 80% thickness (this resembles Case (1)). The initial yielding pressure in FEA is just 8.04MPa while the collapse pressure is much larger as 10.43MPa. This large discrepancy for the

$e=1$ here has not been observed for the case (1) where $e=0$. So this delicate analysis shows the meaning of this investigation on the effect of e . The deformed configuration is shown in Fig.S7 (displacements are amplified by a factor 10 to make visualization easier). And the stress distribution is quite non-uniform and quite different from that in Fig.S4. The corresponding theoretical results are shown in Fig.S8. When maximum stress reaches 239.8MPa, the corresponding pressure is 8.0MPa which result is consistent to the counterpart FEA result 8.04MPa. The theoretical distribution of $\sigma(s)$ is much more non-uniform when Fig.S4 is compared. If initial yielding criterion is used for $e=1$ case, the predicted critical pressure is 8.0MPa which significantly underestimates the collapse pressure 10.43MPa in FEA. So initial yielding criterion is not suitable for $e=1$. We may use Fatt's full plastic criterion (Fatt, 1999) instead to reflect the plasticity effect more accurately: pressure is critical once the equation $|M|/M_0 + (N/N_0)^2 = 1$ is satisfied where M is cross-section resultant moment, M_0 is fully plastic cross-section moment, N is membrane force, N_0 is the fully plastic resultant cross-section force. By adapting this criterion to our case, at critical cross-section $s=0$, $M = EI_1(w_1'' + v_1')$ for $s=0$ and $M_0 = 1/4 \cdot \sigma_y t_1^2$, $N = p(R_1 + t_1/2)$, $N_0 = \sigma_y t_1$. By inserting the theoretical solutions for different p , this equation is satisfied at $p = 9.7399$ MPa. Compared with collapse pressure 10.43MPa, only relative error of 6.6% exists and may be informative for engineering applications (see Table.S1). Indeed there are many such criteria in literature for accounting for various level of plasticity (Fraldi and Guarracino, 2011; 2013) and initial yielding criterion or fully plastic criterion is not the only choice. But from this example, we have just showed how engineering application is possible by using elastic data from theoretical formulation and plastic criterion to predict critical pressure. And Fatt (1999) has used this similar method to predict the critical external pressure of corroded ring based on pure elastic solution too. The main difference is that Fatt studied the special case $e=0$, but we presented more general results for all $e \in [-1,1]$. The above comparison between the $e=0$ and $e=1$ cases has clearly shown the significant effect of e and this is also the main motivation of this paper.

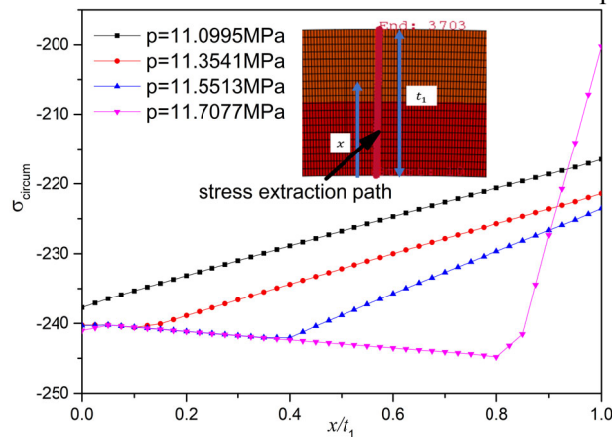


Fig. S5 Stress when collapse pressure is approached at cross-section $s=0$ (crown point) from FEA

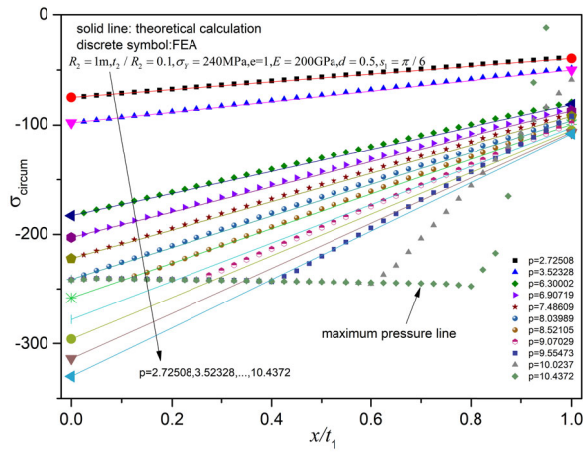


Fig. S6 Stress for $e=1$ case at cross-section of $s=0$

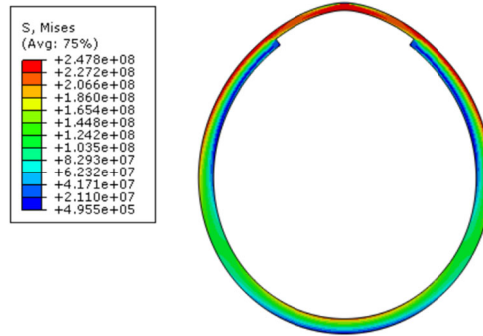


Fig. S7 Mises stress distribution at collapse pressure 10.43MPa in FEA

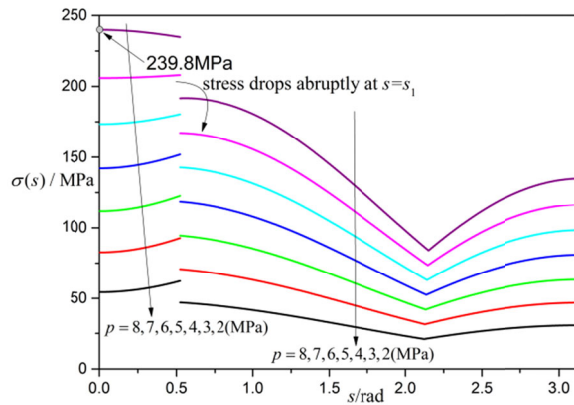


Fig. S8 Stress distribution when $e=1$ (theoretical)

Table. S1 Collapse pressures for FEA and analytical results

Cases	FEM	Analytical	Relative Error
Case 1: $e=0$	11.70MPa	11.53MPa	1.45%
Case 2: $e=1$	10.43MPa	9.74MPa	6.61%

Affiliated Figures

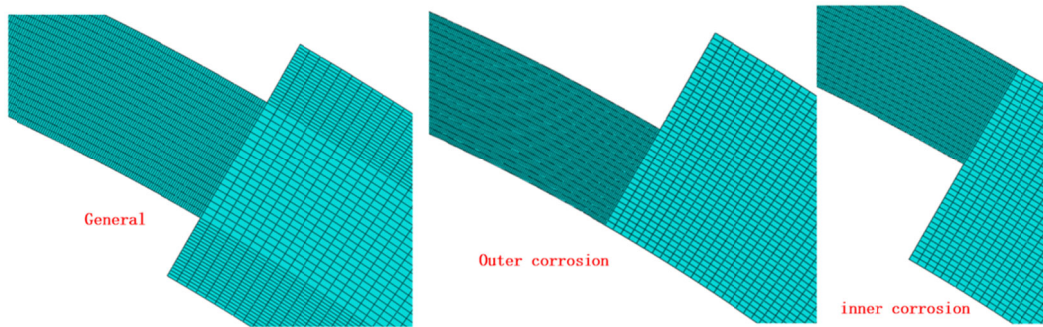


Fig. S9 Meshes around s_1

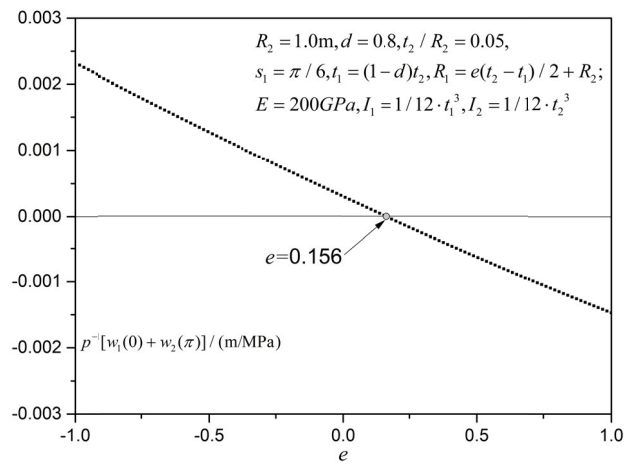


Fig. S10 Initial slope

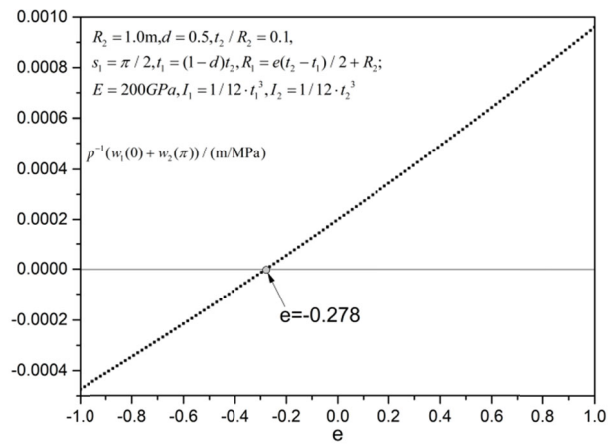


Fig.S11 Initial Slope

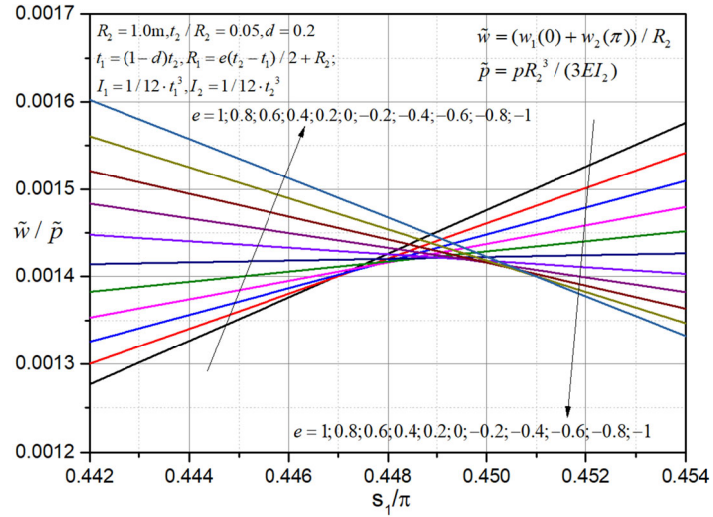


Fig.S12 Amplified plots at $s_1=0.45$ for $d=0.2$

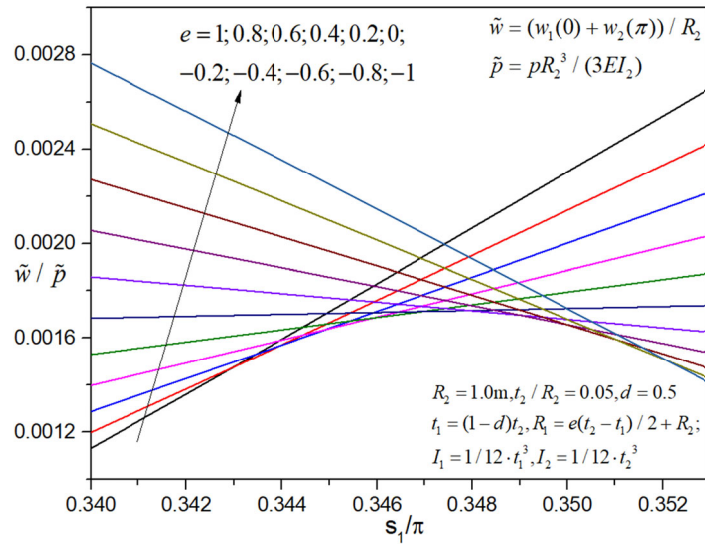


Fig. S13 Amplified plots at $s_1=0.35$ for $d=0.5$

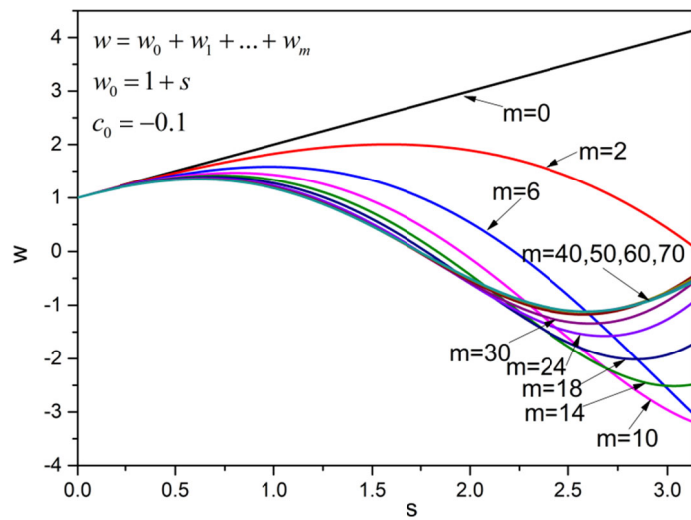


Fig.S14 Slow convergence when $c_0=-0.1$

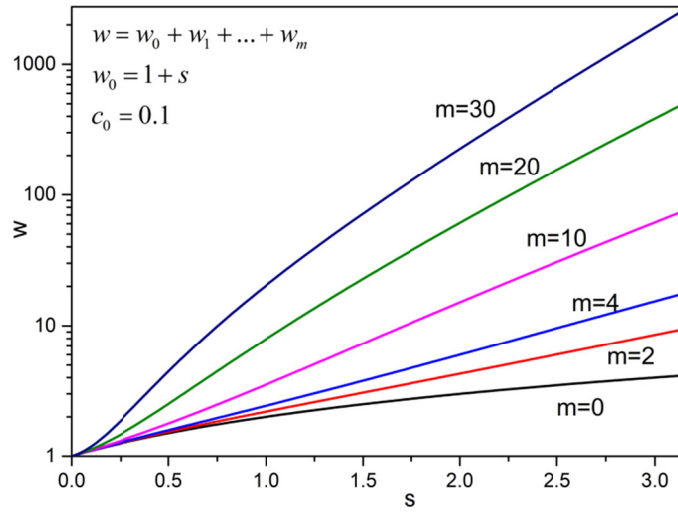


Fig.S15 Rapid divergence when $c_0=0.1$

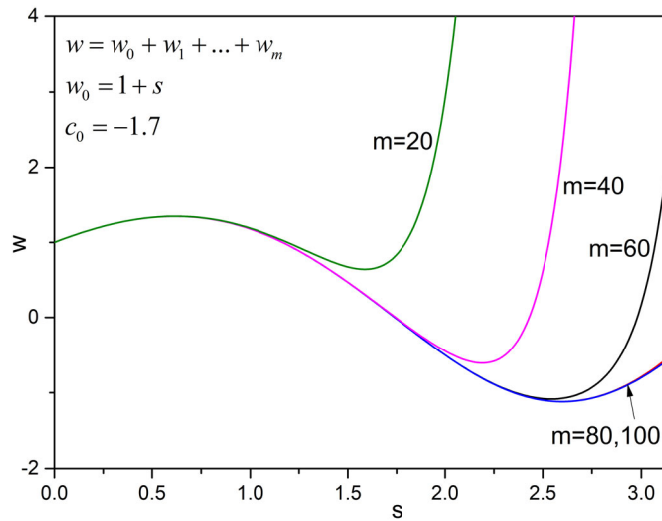


Fig.S16 Slow convergence when $c_0=-1.7$

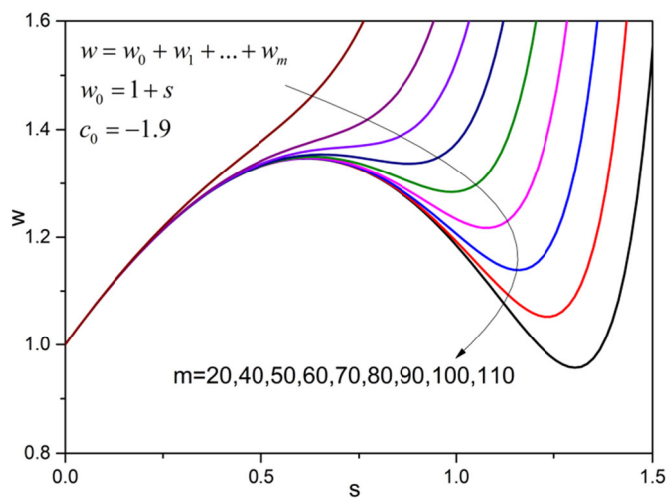


Fig.S17 Extremely slow convergence when $c_0=-1.9$

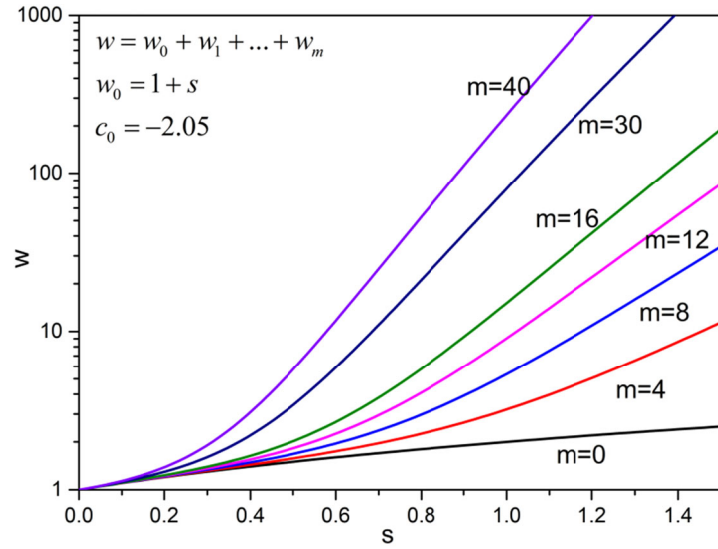


Fig.S18 Rapid divergence when $c_0=-2.05$

Table S2. Comparison of bifurcation pressures

e	simplified1	full1	error1/%	simplified2	full2	error2/%	simplified3	full3	error3/%
1	0.2225	0.2221	-0.1954	0.0809	0.0809	-0.0218	0.8095	0.8094	-0.0127
0.8	0.2250	0.2246	-0.1551	0.0836	0.0835	-0.0159	0.8113	0.8112	-0.0104
0.6	0.2274	0.2272	-0.1160	0.0864	0.0863	-0.0107	0.8131	0.8130	-0.0078
0.4	0.2299	0.2298	-0.0765	0.0893	0.0893	-0.0064	0.8149	0.8148	-0.0053
0.2	0.2325	0.2324	-0.0383	0.0923	0.0923	-0.0028	0.8167	0.8167	-0.0027
0	0.2351	0.2351	0	0.0956	0.0956	0	0.8185	0.8185	0
-0.2	0.2377	0.2378	0.03743	0.0989	0.0989	0.0021	0.8203	0.8203	0.0028
-0.4	0.2404	0.2406	0.07444	0.1024	0.1024	0.0039	0.8221	0.8221	0.0056
-0.6	0.2432	0.2434	0.1114	0.1061	0.1061	0.0047	0.8239	0.8239	0.0085
-0.8	0.2459	0.2463	0.1471	0.1099	0.1099	0.00455	0.8256	0.8257	0.0115
-1	0.2488	0.2492	0.1832	0.1140	0.1140	0.00526	0.8274	0.8276	0.0146